ACS Catalysis

Research Article

pubs.acs.org/acscatalysis

Insights Into the Oxygen Reduction Reaction Activity of Pt/C and PtCu/C Catalysts

Eric J. Coleman, Muntasir H. Chowdhury, and Anne C. Co*

Department of Chemistry and Biochemistry, The Ohio State University, 100 West 18th Avenue, Columbus, Ohio 43210, United States

ABSTRACT: A mechanistic electrochemical study of the oxygen reduction reaction (ORR) on a carbon-supported PtCu catalyst is presented. The catalyst was prepared by galvanic displacement of nanoporous copper with Pt. The electrochemistry of the catalyst was explored at pH 1 and pH 13. Hydrogen peroxide reduction and rotating ring−disk electrode (RRDE) studies showed that the PtCu/C catalyst facilitates a $4e^-$ direct or series reduction to water in alkaline electrolyte. A Tafel study suggests that the ORR rate-limiting step for PtCu/C does not change when the catalyst is subject to pH extremes. The ORR activity of the PtCu/C catalyst was found to be 2−3 times higher than the ORR activity of commercially available Pt/C (Johnson Matthey). Adsorption of OH^- was quantified for PtCu/C and Pt/C, and PtCu/C was observed to have a reduced affinity toward OH_{ads} in both acid and alkaline electrolyte, which was found to promote the rate of the ORR relative to Pt/C. On the basis of this study, we propose that (1) each Pt-based catalyst has a unique rate of change of OH_{ads} coverage which is correlated to its ORR activity and (2) all Pt-based catalysts have the same rate of change of OH_{ads} coverage during irreversible oxide formation.

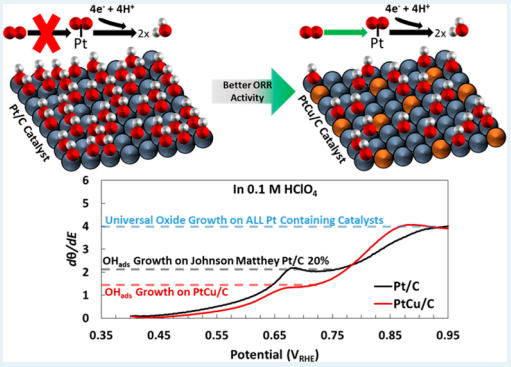

KEYWORDS: *oxygen reduction, electrocatalysis, nanoporous metals, PtCu, Tafel, mechanism*

INTRODUCTION

The oxygen reduction reaction (ORR) is one of the key reactions in fuel cells and metal−air batteries. Despite vast efforts in the past decades to develop non-Pt-based catalysts, Pt remains the catalyst of choice for ORR in aqueous medium. Recently, alkaline electrolytes have been gaining interest due to the general enhanced stability of catalysts under basic conditions, the absence of specific adsorption of spectator ions present in acidic medium, and the possibility of using non-noble-metal catalysts.[1−7]

Significant progress toward the development of cathode catalysts has been made through the efficient utilization of Pt by creating nanoparticles,[8−14] decorating Pt nanoparticles on carbon nanotubes, Au and Pd alloy substrates,[15−19] core−shell catalysts,[6,7,9,20−33] and Pt-based alloys.[6,7,10,12,21−30] The surface electrochemistry of PtX alloys, typically involving 3d transition metals (X = Fe, Ni, Co, Cu)[6,7,10,12,21−30,34] is of great interest due to their enhanced surface activity toward the electrochemical reduction of O_2 (ORR) in comparison to polycrystalline Pt. Nanoparticles and core−shell (core = Ni, Co, Au, Pd, Cu, PtX; shell = Pt) studies suggest that a very thin Pt surface layer introduces lattice strain to the Pt shell which increases the overall ORR activity according to both experiment and theory.[20] Pt−Cu core−shell nanoparticles with improved ORR activity over commercial Pt catalysts has been reported by our group as well as others.[6,7,33] PtCu has also been used in heterogeneous catalysis for CO oxidation,[35] in the dehydrogenation of paraffins,[36] in the synthesis of methyl isobutyl ketone,[37] and as a material for sensors.[38]

In the present study, we investigated the ORR activity of a carbon-supported PtCu structure prepared by galvanically displacing Pt on a tunable nanoporous Cu support made by dealloying Cu alloys. We have previously reported ORR activities of these PtCu catalysts in acidic solution with over 4-fold activity enhancement in comparison to commercially available Pt black (Johnson Matthey) catalysts.[39] This report examines the surface electrochemical processes, for example, the effect of O/OH coverage, which leads to the enhanced activity of this new class of material in comparison to Pt/C. In this report we will focus on the activity of carbon-supported PtCu in alkaline solution (0.1 M KOH) and the comparison of its activity to acidic medium (0.1 M $HClO_4$). We present a detailed analysis of the electrochemical evolution of the catalyst's surface, kinetic parameters for the ORR, the effects of reversible and irreversible surface oxygenation, and the observed pH independence of the rate-limiting step for the ORR.

EXPERIMENTAL SECTION

Nanoporous Copper Synthesis. An AlCu alloy (83 atom % Al) was prepared from bulk high-purity (99.9%) metals at The Ohio State University Solidification and Metal Casting Laboratories (OSU foundry). The alloy was cut into

Received: November 7, 2014
Revised: January 7, 2015
Published: January 7, 2015

DOI: 10.1021/cs501762g
ACS Catal. 2015, 5, 1245−1253

"coins" (24 mm diameter × 2 mm thick). The nanoporous Cu (npCu) structure was created by etching AlCu alloys in NaOH (6 M, at 80 °C for 16 h), followed by continuous rinsing in ultrapure water (>2 h) to remove residual solvent and byproducts. The npCu was dried and stored in a desiccator soon after preparation. The absence of Al in the final porous structure was confirmed by EDX and XPS (negligible signals below the detection limit). Prior to its use as an ORR catalyst support, npCu was heated under an H_2 atmosphere (2 h at 450 °C), to ensure the reduction of any formed Cu oxides (during the etching and storage process) to Cu metal.

Thin-Layer Pt-npCu Electrode Preparation. Following heat treatment of the npCu in H_2, the reduced copper coin was ground into a fine powder using a mortar and pestle. A 7.5 mg portion of npCu powder was added to 7.5 mg of Vulcan XC-72 carbon, and the mixture was dispersed ultrasonically in 10 mL of ultrapure H_2O for 10 min. A diluted Nafion solution (5 wt %, Alfa Aesar, 40 μL) was added to the npCu dispersion. The resulting solution was sonicated for another 10 min. Immediately following sonication, 20 μL of the suspension was drop-casted onto a mirror polished glassy carbon (GC) disk electrode (Pine, 5 mm diameter). The prepared electrode was dried under vacuum (55 °C for 1.5 h). After drying, the coated electrode was cooled to room temperature. For comparison, Pt/C was prepared by dispersing 15 mg of 20 wt % Pt/C (Johnson Matthey 20 wt % on Vulcan XC-72) in 10 mL of ultrapure H_2O for 10 min. There were no other variations from the prior procedure.

Deposition of Pt. A 120 mL portion of a 1.2 mM K_2PtCl_4 (Sigma-Aldrich) solution (ultrapure H_2O from Milli-Q 18.2 MΩ) was added to a standard three-electrode cell with heating jacket. The cell was thermostatically controlled at 50 °C. The nanoporous copper-coated GC electrode was attached to a Pine electrode rotator and immersed in the K_2PtCl_4 solution for 2.5 min. To ensure uniform deposition of platinum, the electrode was rotated at 500 rpm during deposition. Immediately after the timed deposition, the electrode was removed from the platinum solution and rinsed in 200 mL of ultrapure water for 2 min at 500 rpm, twice, to quench the reaction.

Electrochemical Study. Electrochemical measurements were performed in a jacketed standard three-electrode cell using a ring−disk electrode rotator (Pine) equipped with a CH Instruments bipotentiostat (CH 760D) capable of concurrent rotation control. A reversible hydrogen electrode (RHE) with a Luggin capillary was used as the reference electrode for all electrochemical measurements. The counter electrode was a Pt mesh. The electrolyte used was 0.1 M $HClO_4$ or 0.1 M KOH. The 0.1 M $HClO_4$ solution was prepared by diluting concentrated trace metal grade acid (Fisher) with ultrapure deionized H_2O. The 0.1 M KOH solution was prepared by dissolving KOH pellets (Sigma-Aldrich, ACS grade) in ultrapure deionized H_2O. All cyclic voltammograms were recorded at 298 K with a scan rate of 10−100 mV s^{-1} and a rotation rate of 0−1600 rpm. The prepared electrodes were transferred to the electrochemical cell and immersed in nitrogen-saturated electrolyte, deareated for at least 45 min. The electrodes were "acid washed" via electrochemical dealloying using a modification of the method first described by Koh and Strasser.[40] The potential was cycled 50 times between 0.5 and 1.2 V at 1 V/s in 0.1 M $HClO_4$ solution to dealloy and stabilize the catalyst. Then CV scans between 0.03 and 1.2 V at 20 and 100 mV/s were measured until a steady-state voltammogram was attained. The Pt electrochemical surface area (Pt ECSA) was determined from a N_2-saturated voltammogram via the average integrated charge of the underpotentially deposited hydrogen (H_{upd}) region ($0.05 < E < 0.45$ V for acid and $0.05 < E < 0.45$ V for base) after double-layer correction. The widely accepted conversion of 210 μC cm_{Pt}^{-2} for polycrystalline Pt was assumed. ORR CV measurements were performed in an oxygen-saturated electrolyte (0.1 M $HClO_4$ or 0.1 M KOH) with the potential cycled between 0.03 and 1.2 V at 20 mV/s. Polarization curves were obtained by subtracting the N_2-saturated voltammogram from the O_2-saturated voltammogram to remove background contributions. Kinetic ORR activity (i_k) was calculated for the *anodic sweep* polarization curve via the relationship

$$i_k = \frac{i_d i_{tot}}{i_d - i_{tot}} \quad (1)$$

where i_d is the diffusion-limited current and i_{tot} is the total current. Pt specific activities were determined from Pt-ECSA data as follows:

$$\text{specific activity} = \frac{i_k}{\text{Pt ESCA}} \quad (2)$$

Hydrogen peroxide production during ORR was measured via a rotating ring−disk electrode (RRDE, Pine) with a Pt ring electrode held at 1.2 V vs RHE during the measurement of the ORR on the disk. The RRDE experiments were conducted in O_2-saturated 0.1 M $HClO_4$ or 0.1 M KOH at room temperature. Before the ORR RRDE scan, a potential hold was measured at the ring in the absence of an applied potential at the disk to establish a background current. The ring background current was subtracted from the peroxide oxidation ring current. The collection efficiency, N, for the RRDE was 0.28. All electrochemistry experiments were repeated at least four times to ensure reproducibility.

Hydrogen peroxide reduction was measured independently with the PtCu/C catalyst on the disk electrode by diluting a 30% hydrogen peroxide (Fisher, ACS grade) solution to 5×10^{-4} M in 0.1 M KOH electrolyte. CV scans were obtained between 0.03 and 1.2 V at 20 mV/s and rotation rates varying between 500 and 1600 rpm.

Electrochemical impedance spectroscopy (EIS) was measured to determine the solution resistance for the electrochemical system to correct for IR loss, using a Princeton Applied Research 263A potentiostat in conjunction with a Solartron 1260 Impedance Analyzer. The impedance was measured at OCP and at 0.9 V (amplitude of 5 mV from 10000 to 0.01 Hz). The correction was applied to raw data as follows:

$$E_{real} = E_{measured} - E_{IR} \quad (3)$$

RESULTS AND DISCUSSION

Electrochemical Behavior of Pt-npCu/C in 0.1 M KOH. As previously reported by our group,[39] fresh galvanically displaced Pt-npCu/C occasionally results in residual Cu on the surface of Pt, the amount of which depends on the displacement conditions. Figure 1A shows the electrochemical features of a freshly deposited Pt-npCu reaching a steady state within 16 potential cycles in N_2-deaereated 0.1 M KOH. A comparison of the voltammograms between freshly displaced Pt-npCu/C and Pt-npCu/C after acid washing is given in Figure 1B. Freshly deposited Pt-npCu/C (Figure 1A) typically shows a slightly distorted H_{upd} feature in the region $0.4 < E < 0.05$ V. Oxidative and reductive peaks in the region between 0.50 and 0.9 V could

DOI: 10.1021/cs501762g
ACS Catal. 2015, 5, 1245−1253

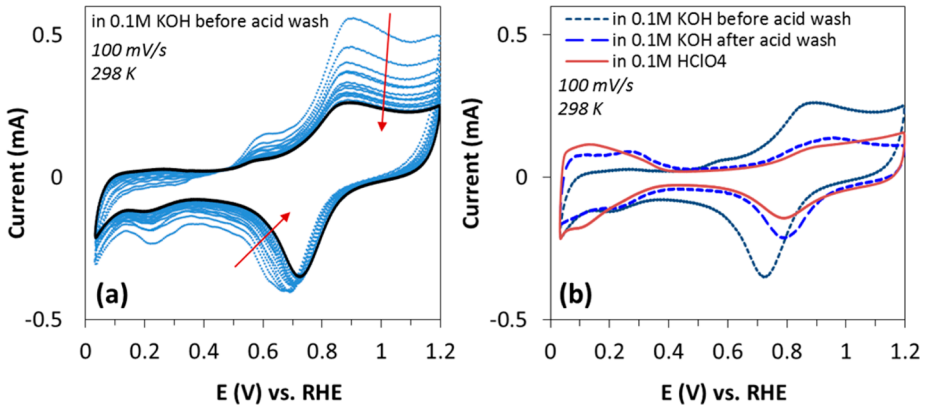

Figure 1. Cyclic voltammograms (CVs) of a freshly displaced Pt-npCu/C catalyst: (a) the initial 16 cycles in N_2 deaerated 0.1 M KOH; (b) steady state CVs recorded (1) in base, (2) after 50 cycles 0.6–1.2 V (1 V/s) in acid, and (3) again in base.

be from a combination of Cu oxidation/reduction among Cu, Cu_2O, and $Cu(OH)_2$ and Pt oxidation/reduction between Pt^0 and platinum oxide/hydroxides. The literature has reported possible dissolution of Cu_2O to $HCuO_2^-$ at pH 13 during the anodic sweep, which can be redeposited back to the electrode upon the cathodic sweep.[7]

On the other hand, residual Cu species on the surface dissolve readily in acid. After being subjected to acid washing, Pt-npCu/C catalysts measured in both 0.1 M $HClO_4$ and 0.1 M KOH show classical Pt features and Pt oxidation and reduction peaks at ca. 0.8 V, indicative of exposed Pt at the surface layer. Unless specifically stated otherwise, ORR studies in both acid and alkaline electrolytes reported in this paper were measured after residual Cu was removed upon cycling in acid (ca. 50 cycles at 1 V/s between 0.6 and 1.2 V) until a steady-state voltammogram and ECSA were obtained. The acid-washed catalysts from here on will be referred to as PtCu/C.

ORR Activity and H_2O_2/HO_2^- Detection on PtCu/C. In both 0.1 M $HClO_4$ and 0.1 M KOH solutions, the oxygen reduction reaction is generally described as having three regions: the kinetically controlled region (>0.85 V) and combined kinetic–diffusion control (0.6 < E < 0.85 V), followed by a well-defined diffusion-limiting current indicating the ORR is purely transport controlled at <0.6 V. The kinetics of the reduction of O_2 are known to be different under different sweep directions for Pt-based catalysts.[41] The voltammetric curves recorded in the anodic (positive) sweep represent O_2 reduction on an essentially oxide-free surface, while during the cathodic (negative) sweep the reaction occurs on partially oxidized surfaces. The most recent convention is to compare the ORR activity of Pt-based catalysts via the anodic sweep, assuming an oxide-free surface. Unless otherwise stated, oxygen reduction and hydrogen peroxide reduction/oxidation polarization curves presented in this paper were anodic sweeps only. The ORR polarization curves were obtained by subtracting the background current caused by capacitance and surface processes on the electrode (measured in N_2) from the O_2-saturated voltammogram. ORR polarization curves (before subtraction), along with their associated background currents, are shown in Figure 2 for the PtCu/C catalyst in 0.1 M $HClO_4$ and in 0.1 M KOH.

Hydrogen peroxide produced during the course of the ORR was detected in the corresponding ring current where the ring potential was held constant at 1.2 V, such that peroxide oxidation occurred under diffusion control. The percent peroxide production can be calculated from the ring–disk measurement

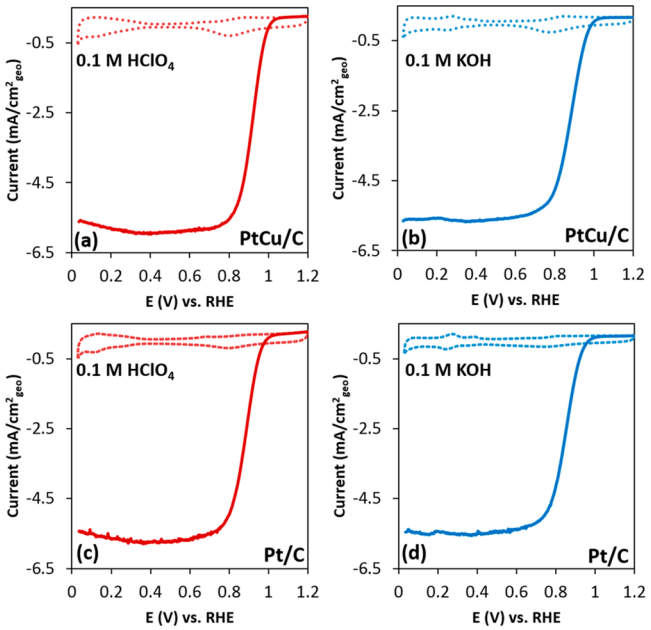

Figure 2. CV of acid-washed PtCu/C in N_2-deaerated electrolyte along with anodic scan of PtCu/C in O_2-saturated electrolyte. Electrolytes are (a) 0.1 M $HClO_4$ and (b) 0.1 M KOH. Corresponding CVs of Pt/C (Johnson Matthey 20 wt % on Vulcan XC-72) are shown in (c) and (d) for acid and base electrolytes, respectively. All electrochemical measurements were performed at 20 mV/s, 1600 rpm, and 298 K.

according to the following equation, where the collection efficiency, N = 0.28:

$$x\mathrm{H_2O_2}\ (\%) = \frac{I_{\mathrm{ring}}}{I_{\mathrm{disk}}N} \times 100 \qquad (4)$$

Figures 3 and 4 show that ORR on PtCu/C in both 0.1 M $HClO_4$ and 0.1 M KOH proceeds entirely through a four-electron pathway. The amount of peroxide produced on the PtCu/C catalyst (Figure 3) is essentially negligible throughout the potential region between 0.9 and 0.2 V in base and between 0.9 and 0.4 V in acid. Detectable H_2O_2 production in the region of H_2 desorption, below ~0.4 V in acid, indicates that a surface covered with hydrogen adatoms may facilitate the formation of peroxide. Interestingly, the as-prepared Pt-npCu/C, which contains residual surface Cu, did not produce any detectable

DOI: 10.1021/cs501762g
ACS Catal. 2015, 5, 1245–1253

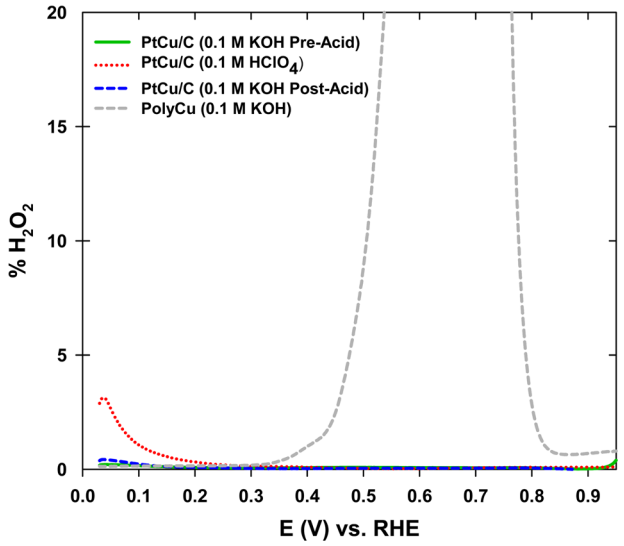

Figure 3. H_2O_2 formation measured from Pt ring held at 1.2 V during ORR anodic sweep for PtCu/C and polycrystalline Cu catalysts in 0.1 KOH and 0.1 M $HClO_4$. The disk electrode was swept from 0.03 to 1.2 V at a rotation rate of 1600 rpm and 25 °C.

peroxide during the ORR, whereas on a monometallic polycrystalline Cu surface, the ORR clearly goes through a $2e^-$ reduction process, producing predominantly H_2O_2 between 0.8 and 0.3 V.

The four-electron ORR pathway for PtCu/C in alkaline solution can also be confirmed via analysis of Levich plots of the anodic sweeps from 0 to 1.2 V

$$\frac{1}{i_{tot}} = \left(\frac{1}{i_k} + \frac{1}{i_d}\right) = \left(\frac{1}{i_k} + \frac{1}{B}\omega^{-1/2}\right) \quad (5)$$

$$i_d = 0.62nFD^{2/3}\nu^{-1/6}C\omega^{1/2} = B\omega^{1/2} \quad (6)$$

where n, F, D, ν, C, and ω are the total number of electrons, Faraday constant, diffusion coefficient (cm^2/s), kinematic viscosity (cm^2/s), concentration (mol/cm^3), and rotation rate (rad/s), respectively. Figure 4b shows the Levich plot (i^{-1} vs $\omega^{-1/2}$) for ORR in alkaline solution at various potentials ranging from 0.8 to 0.2 V. The B factor obtained from the slope of a Levich plot was $[9.1(\pm 2)] \times 10^{-2}$ mA $rpm^{-1/2}$, which agrees with a theoretical four-electron-reduction process (3.99×10^{-2} mA $rpm^{-1/2}$) from 0.8 to 0.2 V, calculated with literature data for O_2 concentration of 1.21×10^{-6} mol/cm^3, kinematic viscosity (ν) of 1.008×10^{-2} cm^2/s, and O_2 diffusivity of 1.86×10^{-5} cm^2/s in 0.1 M KOH at 293 K.[41] The intercepts of the Levich plot correspond to the kinetic currents, and it is also noteworthy that at potentials <0.6 V the plot intercepts i^{-1} at the origin, proving that the current at potentials <0.6 V is diffusion limited. Consistent with our ring data, Pt-npCu/C (which may contain surface Cu residue) also suggests a four-electron-reduction pathway in alkaline solution, as shown in the Levich plot in Figure 4b.

H_2O_2 Reduction Reaction on PtCu/C. Hydrogen peroxide reduction was conducted on the PtCu/C catalyst in a solution free of oxygen to simulate the chemical environment when H_2O_2 is produced as an intermediate or final product during the O_2 reduction process. Under basic conditions, H_2O_2 dissociates to HO_2^- and H^+ (pK_a 11.6). Figure 5a shows a family of polarization curves for HO_2^- reduction obtained on the PtCu/C catalysts in 0.1 M KOH at varying rotation rates and the corresponding Levich plot. Unlike oxygen reduction/oxidation, the reduction/oxidation process of hydrogen peroxide is highly reversible on PtCu/C, as indicated by the oxidation and reduction currents in Figure 5a and a wide region of well-defined mass transport controlled oxidation and reduction.

The Levich plot in Figure 5b confirms a two-electron reduction and oxidation of H_2O_2 to H_2O and O_2, respectively, assuming a kinematic viscosity of 1.008×10^{-2} cm^2/s, HO_2^- diffusivity of 8.75×10^{-6} cm^2/s in 0.1 M KOH at 293 K, and

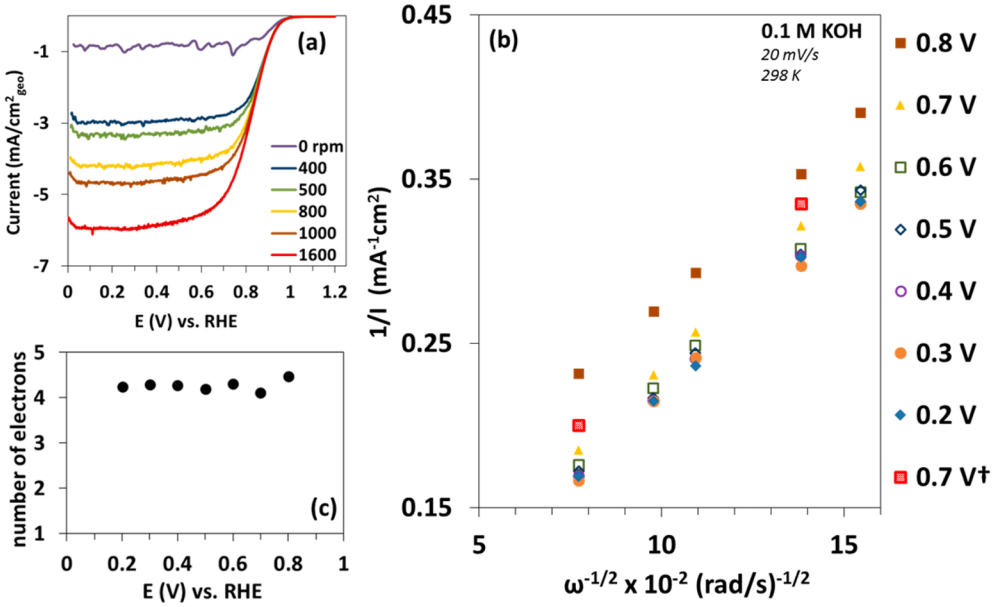

Figure 4. ORR on PtCu/C in 0.1 M KOH: (a) background-subtracted polarization curves (anodic sweep) obtained from CV scans in O_2-saturated electrolyte at rotation rates varying from 0 to 1600 rpm; (b) corresponding Koutecky–Levich plots; (c) number of electrons exchanged for ORR as a function of applied potential, calculated from Koutecky–Levich plots. (†) Data obtained from Pt-npCu/C catalyst in KOH before acid washing (contains regions of exposed copper).

DOI: 10.1021/cs501762g
ACS Catal. 2015, 5, 1245−1253

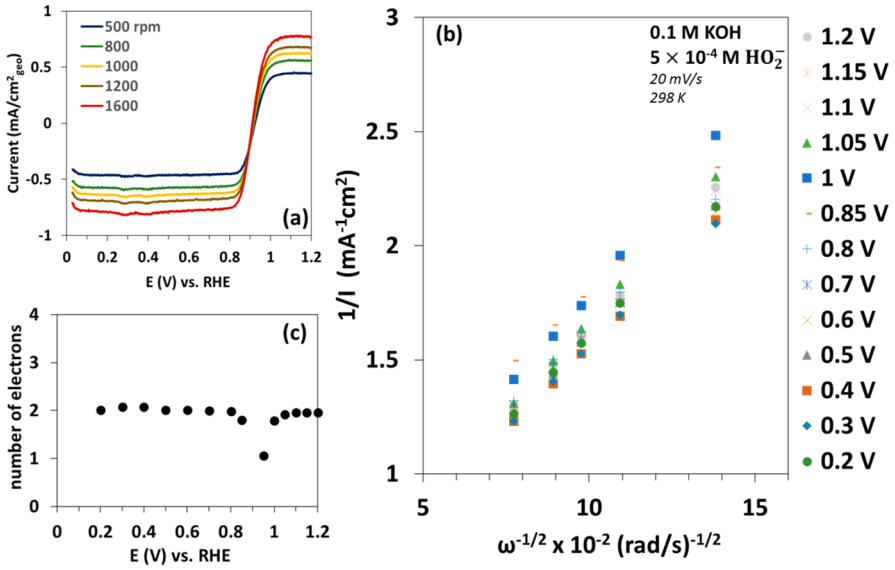

Figure 5. Hydrogen peroxide reduction on PtCu/C in 0.1 M KOH: (a) background-subtracted polarization curves (anodic sweep) obtained from CV scans at rotation rates varying from 0 to 1600 rpm; (b) corresponding Koutecky–Levich plots; (c) number of electrons exchanged for hydrogen peroxide reduction as a function of applied potential, calculated from Koutecky–Levich plots.

a peroxide concentration of 5×10^{-4} M. Except for $0.9 < E < 0.95$ V, the Levich plot between 0.2 and 1.2 V intercepts the origin, indicating a pure mass transfer control of the peroxide reaction over a wide range of potentials.

A comparison of the ORR polarization curve to the hydrogen peroxide polarization curve is shown in Figure 6. The overpotential

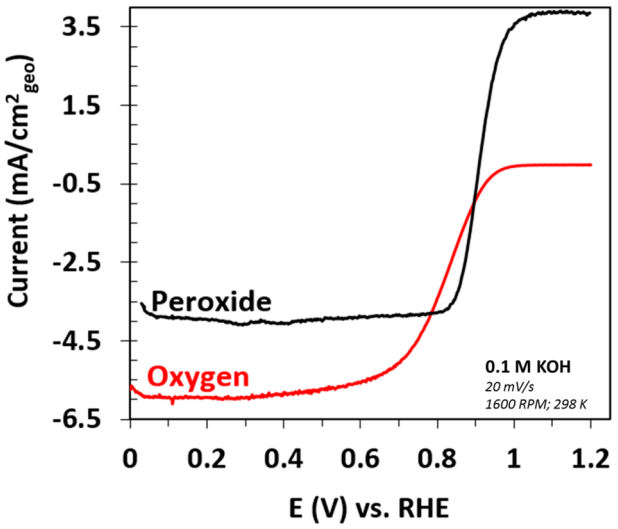

Figure 6. Polarization curves of ORR and peroxide reduction for PtCu/C in 0.1 M KOH (anodic scans only).

for hydrogen peroxide reduction on PtCu/C is smaller than that of the oxygen reduction on PtCu/C, indicating that, if peroxide is formed as an adsorbed intermediate of the ORR, it could be electrochemically reduced immediately to H_2O. This finding is consistent with the observed overall $4e^-$ reduction of O_2 on PtCu/C, and it suggests that ORR on PtCu/C in 0.1 M KOH could occur through a $4e^-$ series pathway or a one-step direct pathway (from O_2 to H_2O).

$$O_2 \xrightarrow{2e^-} HO_2^- \xrightarrow{2e^-} H_2O \quad (4e^- \text{ overall}) \tag{7}$$

Tafel Analysis and Effect of OH_{ads}. To provide further insight into the mechanistic pathway of the ORR, Tafel plots showing mass transport corrected ORR current densities (anodic sweep) for PtCu/C after acid washing are presented in Figure 7. For PtCu/C, one may extrapolate a line at low current densities (lcd; defined as spanning the range of potentials where the kinetic current is between 0.25% of the limiting current and where the Tafel line begins to deviate from linearity), giving Tafel slopes of ~50 mV/dec in acid and base. A line can also be extrapolated for higher current densities (hcd; defined as the linear Tafel range between the lcd Tafel region and the diffusion-limited current region), giving Tafel slopes of ~90 mV/dec of i in base and ~80 mV/dec of i in acid. The similarity of the lcd and hcd Tafel slopes at the two extreme pHs suggests that the rate-limiting steps (RLS) of the ORR on PtCu/C are the same, regardless of pH. Moreover, the Tafel slopes over the entire current range for PtCu/C are very similar to the associated Tafel slopes for Pt/C (Johnson Matthey 20 wt % on Vulcan XC-72), indicating that the mechanistic pathway for ORR on PtCu/C is very similar to the pathway on commercially available Pt/C.

There is a general consensus that the ORR rate-limiting step for Pt catalysts, regardless of current density, involves electron transfer to $O_{2,ad}$.[41,42] The change in Tafel slope from ~50 to >85 mV/dec is not linked to a change in the RLS but is attributed to differences in adsorption of oxygen-containing species. These adsorbates are generally believed to be attributed to (1) ORR reaction intermediates[43] or (2) chemisorbed hydroxyl groups (OH_{ads}) from the electrolyte.[41,44] Both theories hold that the change in Tafel behavior is primarily related to a marked change in electrode adsorbate coverage. However, it has been very difficult for any research group to provide conclusive findings that completely deconvolutes the entire ORR mechanistic pathway, particularly on a polycrystalline Pt-based catalyst material.

Regardless, most reports of ORR on Pt surfaces under acidic and alkaline conditions imply that OH_{ads} blocks active sites for electron transfer to O_2.[44] Moreover, studies by Markovic et al. show that the activity of Pt is essentially dependent on structure

DOI: 10.1021/cs501762g
ACS Catal. 2015, 5, 1245–1253

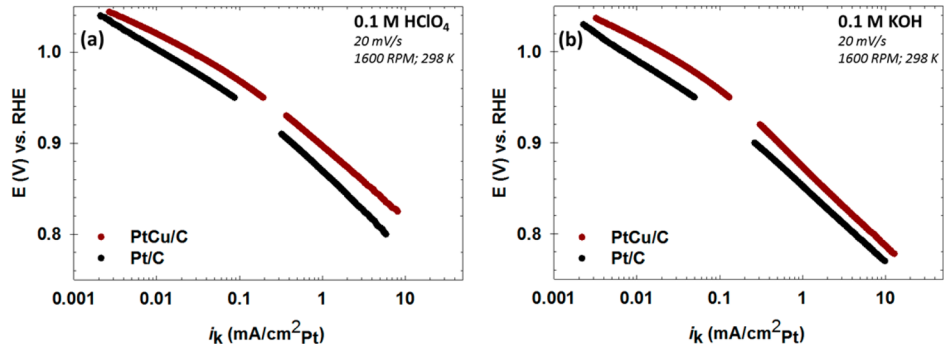

Figure 7. Tafel plot of specific kinetic current density during ORR for PtCu/C and Pt/C (Johnson Matthey 20 wt % on Vulcan XC-72) catalysts in (a) 0.1 M $HClO_4$ and (b) 0.1 M KOH after acid washing. Conditions: O_2 saturated; anodic sweeps only; mass transport and IR corrected.

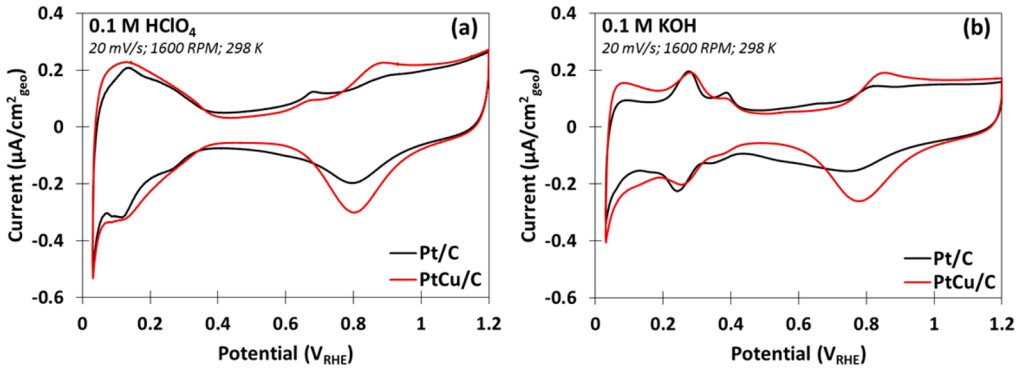

Figure 8. Comparison of background CVs for PtCu/C and Pt/C (Johnson Matthey 20 wt % on Vulcan XC-72) in N_2-dearated (a) 0.1 M $HClO_4$ and (b) 0.1 M KOH.

sensitive adsorption of OH on the various Pt(hkl) facets,[45] with the lowest OH_{ad} coverage on Pt(111) correlating to the highest activity (in alkaline solution).[40,44]

To present a more concrete depiction of the effect of OH_{ads} coverage on the catalyst surface, we will endeavor to quantify OH_{ads} coverage on PtCu/C relative to Pt/C. We will proceed by accepting the hypothesis that, for hydrogen adsorption/desorption on a polycrystalline Pt surface, ~210 $\mu C/cm^2_{Pt}$ corresponds to a full monolayer coverage ($1e^-$ per Pt atom).[46] Next, we assume that pseudocapacitance from hydrogen adsorption/desorption occurs only at potentials of $0.05 < E < 0.4$ V in 0.1 M $HClO_4$ and $0.05 < E < 0.45$ V in 0.1 M KOH. On the basis of the overlap in the blank and ORR CVs for $E > 0.95$ V shown in Figure 2, we will also assume that OH_{ads} coverage at all potentials is unchanged by the presence of O_2. Finally, we assume that the double-layer capacitance from the carbon support is constant over the potential range $0 < E < 1.2$ V. Thus, at potentials more positive than 0.4 V (acid) or 0.45 V (base), any pseudocapacitive feature must be the result of adsorption/desorption of OH^-,[41,47] on the basis that our experiments are performed in N_2 (or O_2)-purged electrolyte that is not known to adsorb any other spectator anions on the Pt surface.[44] Under these assumptions, we can use the N_2-purged "blank" voltammogram to calculate the effective surface area of the Pt catalyst, using the average charge from adsorption/desorption of the hydrogen monolayer after double-layer correction. Using the anodic sweep of the blank voltammogram, the charge associated with OH_{ads} at potentials >0.4 V in $HClO_4$ and >0.45 V in KOH can then be expressed as

$$Q_{OH_{ads}} = \frac{\int iE\ dE}{v} - Q_{DL} \tag{8}$$

where i is the observed current, v is the sweep rate (0.02 V/s), and Q_{DL} is the total charge associated with the double-layer capacitance. It follows that the coverage of OH_{ads} should then be

$$\theta_{OH_{ads}} = \frac{\frac{Q_{OH_{ads}}}{210\ \mu C/cm^2}}{\text{Pt area}} = \frac{Q_{OH_{ads}}}{Q_{H_{ads}}} \tag{9}$$

It should be noted that 210 $\mu C/cm^2_{Pt}$ is assumed, which may be the most extreme assumption of this method, but we believe that as long as the same constant is utilized for both H_{upd} and OH_{ads} this assumption can be justified, at least from a qualitative standpoint. Figure 8 shows the blank voltammetry from which $\theta_{OH_{ads}}$ was calculated. Close inspection of this figure will show that both PtCu/C and Pt/C catalysts exhibit similar electrochemical behavior. $\theta_{OH_{ads}}$ as a function of electrode potential is shown in Figure 9. In 0.1 M $HClO_4$, OH_{ads} coverage on PtCu/C is at least 1.5 times less than OH_{ads} coverage on Pt/C at all potentials shown. Similarly, in 0.1 M KOH, OH_{ads} coverage on PtCu/C is at least 2 times less than OH_{ads} coverage on Pt/C. These observations provide some quantitative rationale for the increase in ORR specific activity (@ 0.9 V) for PtCu/C catalysts relative to Pt/C, i.e.

$$\frac{i_k(\text{PtCu/C})}{i_k(\text{Pt/C})} \approx \frac{\theta_{OH_{ads}}(\text{Pt/C@0.55 V})}{\theta_{OH_{ads}}(\text{PtCu/C@0.55 V})} \tag{10}$$

where i_k(PtCu/C) and i_k(Pt/C) are the Pt area based kinetic activities for PtCu/C and Pt/C, respectively. This linear approximation is more accurate for catalysts that were tested under alkaline conditions; in acid, the activity enhancement is

DOI: 10.1021/cs501762g
ACS Catal. 2015, 5, 1245−1253

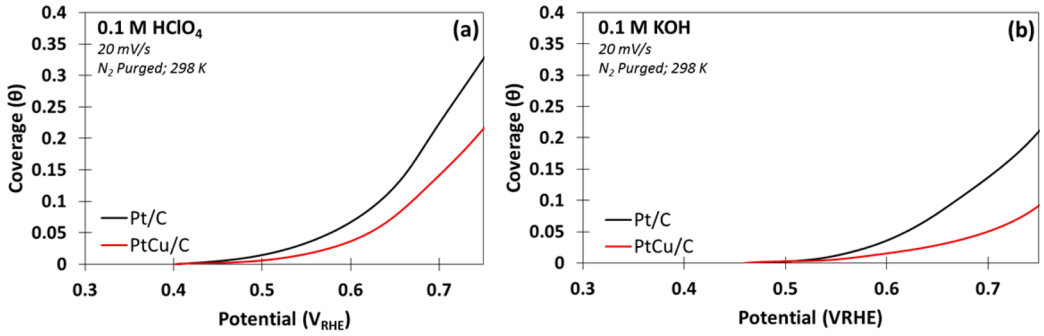

Figure 9. Comparison of reversible OH_{ads} coverage as a function of potential for PtCu/C and Pt/C (Johnson Matthey 20 wt % on Vulcan XC-72) catalysts in (a) 0.1 M $HClO_4$ and (b) 0.1 M KOH, derived from anodic sweep of N_2-deaerated CV.

Table 1. Comparison of OH_{ads} Coverage to Enhancement in ORR Specific Activity

system	reversible OH_{ads} $((\theta_{OH_{ads}@0.55\ V\ Pt/C})/(\theta_{OH_{ads}@0.55\ V\ PtCu/C}))$	irreversible OH_{ads}@ 0.85 V $((\theta_{OH_{ads}@0.85\ V\ Pt/C})/(\theta_{OH_{ads}@0.85\ PtCu/C}))$	irreversible OH_{ads}@ 0.9 V $((\theta_{OH_{ads}@0.9\ V\ Pt/C})/(\theta_{OH_{ads}@0.9\ V\ PtCu/C}))$	$((i_{k@0.85\ V\ PtCu/C})/(i_{k@0.85\ V\ Pt/C}))$	$((i_{k@0.9\ V\ PtCu/C})/(i_{k@0.9\ V\ Pt/C}))$
0.1 M $HClO_4$	2.06	1.21	1.12	2.86	2.82
0.1 M KOH	2.09	1.50	1.33	1.99	2.30

underestimated, but there is still a very strong negative correlation between activity and coverage (Table 1). We believe other related (carbon-supported) bimetallic Pt-based catalysts can be analyzed similarly and their activity (in a given electrolyte/pH) will also scale inversely with the reversible OH_{ads} coverage. Our conclusions here are in agreement with the theory that OH_{ads} is blocking electron access to O_2 and that OH_{ads} determines the activity and mechanistic pathway of the ORR.[34,41,44,45]

Potentials above 0.75 V are omitted in Figure 9 because it is widely believed that the adsorption of OH is no longer reversible at potentials greater than 0.75 V.[41,47] This is illustrated in Figure 8 as the nonsymmetry between anodic and cathodic currents at potentials greater than 0.75 V. However, we believe that the *reversible* OH_{ads} ($0.5 < E < 0.75$ V) coverage and the rate of increase of the reversible coverage ($d\theta/dE$), henceforth called differential coverage, is an intrinsic property of the catalyst material. This hypothesis is illustrated in Figure 10, which shows the differential coverage ($d\theta/dE$) as a function of potential. In both alkaline and acidic electrolytes, there are two plateaus (per catalyst) which correspond to potential regions where the change in $\theta_{OH_{ads}}$ is constant. The lower of the two plateaus at ca. $0.66 < E < 0.74$ V (0.1 M $HClO_4$) and $0.63 < E < 0.70$ (0.1 M KOH) clearly shows that the rate of change of OH_{ads} coverage is higher for Pt/C than for PtCu/C in both electrolytes. Conversely, the higher of the two plateaus at ca. $0.90 < E < 0.95$ V (0.1 M $HClO_4$) and $0.83 < E < 0.90$ V (0.1 M KOH) shows that the two different catalyst surfaces reach the same rate of change of OH_{ads} coverage, $d\theta/dE \approx 4$ in acid, and $d\theta/dE \approx 3.75$ in base. If the coverage is changing by a constant rate of four monolayers per volt, then the catalyst is almost certainly accruing an irreversible layer of oxide, which should be measurable on any platinum surface as a very similar differential coverage. However, the lower plateau on the plot of differential coverage provides the rate at which the reversible OH_{ads} species is adsorbing to a surface, and this quantity is unique for different catalysts. Therefore, at a given pH, the higher of the two plateaus on the plot of differential coverage corresponds to the *universal* rate of growth of an irreversible oxide layer on a Pt-containing surface, whereas the lower plateau is the *intrinsic* rate of growth of the reversible OH_{ads} on the surface of a Pt-containing catalyst.

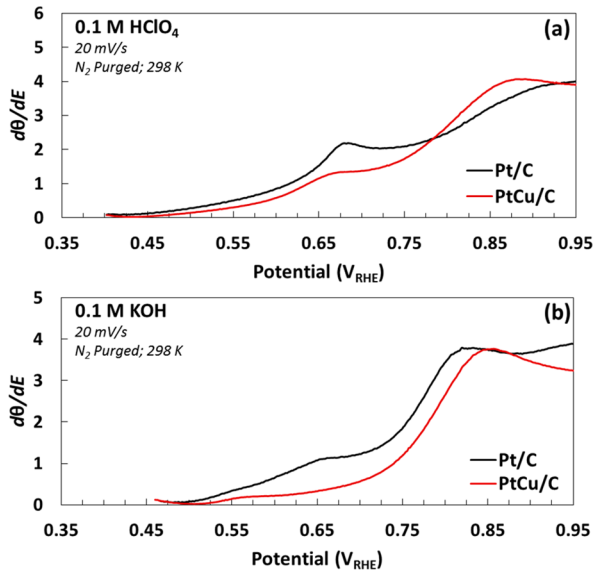

Figure 10. Rate of change of reversible OH_{ads} coverage as a function of potential for PtCu/C and Pt/C (Johnson Matthey 20 wt % on Vulcan XC-72) catalysts in (a) 0.1 M HClO4 and (b) 0.1 M KOH, derived from anodic sweep of N_2-deaerated CV.

It should be stressed that Pt catalysts are not directly comparable unless the electrochemical measurements are performed under the same pH and electrolyte conditions. As of yet, we have been unable to relate the quantified coverage of OH_{ads} across different electrolytes. A manifestation of this can be deduced from Figure 9, where lower OH_{ads} coverage for PtCu/C in base should in principle have better performance in base than in acid, which is not observed. This observation suggests that the oxygen reduction reaction is primarily dictated by its inherent rate, which depends on the electrolyte conditions (i.e., pH in this case), whereas the OH coverage can be used as a descriptor for comparing across materials tested under the same conditions. Further, this method of analysis will only hold for catalysts that (1) are Pt based or (2) have an X@Pt core−shell structure (X = transition metal).

DOI: 10.1021/cs501762g
ACS Catal. 2015, 5, 1245−1253

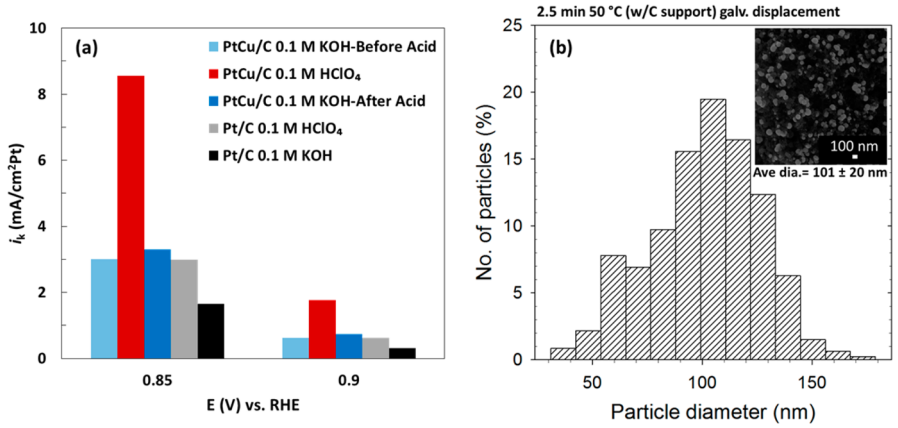

Figure 11. (a) Comparison of ORR specific activity at 0.9 and 0.85 V for PtCu/C and Pt/C (Johnson Matthey 20 wt % on Vulcan XC-72) catalysts, derived from anodic sweeps at 20 mV/s and 298 K, with mass transport and IR correction. (b) Particle size distribution of PtCu/C.

ORR Specific Activity Analysis. While the mechanisms of the ORR may be very similar under acidic and alkaline conditions, the catalytic activities in acid and base are clearly distinct. PtCu/C is most active under acidic conditions, with an onset potential of ca. 1.0 V, in comparison to ca. 0.95 V under alkaline conditions. In the presence of residual Cu on the surface, the onset of ORR occurs at a higher overpotential of ~0.85 V. The specific activity of each catalyst was obtained from the background/mass transport corrected anodic sweep (0 to 1.2 V_{RHE}, 20 mV/s) in O_2-saturated 0.1 M $HClO_4$ and 0.1 M KOH solutions. Figure 11 displays the specific activities at 0.9 and 0.85 V for PtCu/C and Pt/C catalysts (1) before acid cleaning in 0.1 M KOH, (2) in 0.1 M $HClO_4$, and (3) after acid cleaning in 0.1 M KOH. The PtCu/C catalyst, even with regions of exposed Cu, experiences higher activity than Pt/C. The activity enhancement for PtCu/C in comparison to Pt/C is about 3-fold in acid and 2-fold in base. It is worth mentioning that the specific activity of the catalyst in KOH is virtually the same before and after acid cleaning. The surface area of the Pt-npCu/C catalyst is much smaller before cleaning; therefore, we believe that the active catalytic site on both pre- and post-acid-washed surfaces is the same, but there is a higher density of available active sites on the acid-washed catalyst, resulting in a similar specific activity. This observation is in agreement with the ring data for np-PtCu/C in Figure 3 and the Levich plot for PtCu/C in Figure 4.

The high activity of the PtCu/C catalysts is likely the result of two key factors: (1) lattice strain from alloying Pt with Cu and (2) reduced surface affinity toward OH_{ads}. Lattice strain on Pt is generally accepted for providing enhancement of ORR activity on Pt-based bimetallic catalysts,[6,7,30] particularly for core−shell catalysts with a shell thickness of <1 nm. The enhanced activity observed for the PtCu catalysts reported here is due to some contribution from lattice strain[39] on Pt. A measure of the catalyst's oxophilicity is exemplified in its affinity toward OH_{ads} and the ease of oxide/OH_{ads} removal. The change in reversible OH_{ads} coverage per unit change of voltage (Figure 10) is consistently higher for Pt/C than for PtCu/C under both alkaline and acidic conditions, indicating a stronger affinity toward OH_{ads} for Pt/C than for PtCu/C. The oxide removal peak on the reverse sweep also reveals analogous behavior where the reduction of the Pt oxide film on PtCu/C has a 30 mV lower overpotential in comparison to that on Pt/C.[39] The altered oxophilicity of the catalyst may be due to the electronic contributions of the alloying metal, surface structure of the catalyst, and size of the catalyst particles. Our earlier paper reports the effect that the PtCu/C particle size[39] has on the oxophilicity of the surface and its influence on the ORR activity. In this paper, we have observed an inverse correlation between ORR activity and the surface OH_{ads} coverage/affinity. On the basis of our work, it is observed that Pt-based catalysts exhibiting a weaker Pt−O or Pt−OH bond benefit from an ORR activity enhancement.

CONCLUSIONS

Herein, the kinetics of the oxygen reduction reaction was studied on the highly active PtCu/C catalyst at extreme pHs. The initial catalyst structure with exposed copper was introduced, as well as the voltammetric evolution toward the final active form of the catalyst. The catalyst was shown to facilitate either a $4e^-$ direct or series path to water, with almost no measurable peroxide formation at useful potentials. Tafel slopes for the catalyst indicate that the rate-determining step is likely the transfer of the first electron. A detailed look at OH_{ads} provides further verification that OH_{ads} blocks electron access to O_2 and shows that the PtCu/C catalyst has a reduced surface affinity toward OH_{ads} in comparison to Pt/C. On the basis of the OH_{ads} study, it was observed that (1) Pt-based catalyst materials have a unique initial rate of change of OH_{ads} coverage which is directly correlated with their ORR activity and (2) there is a universal rate of change of OH_{ads} coverage (~3.75−4 monolayers per volt) that describes the formation of an irreversible oxide film on any Pt-based catalyst. The electrochemical methods and results described in this work can provide insight into the nature of the ORR activity for Pt-based catalyst materials.

AUTHOR INFORMATION

Corresponding Author

*E-mail for A.C.C.: co@chemistry.ohio-state.edu.

Notes

The authors declare no competing financial interest.

ACKNOWLEDGMENTS

This work was supported by the Department of Chemistry and Biochemistry and also in part by The Ohio State University Graduate Enrichment Fellowship and The Ohio State University Faculty Startup Funds. We also thank Dr. Sarum Boonmee for his generous help with operation of the furnace at the OSU foundry and his preparation of the CuAl precursor alloys.

DOI: 10.1021/cs501762g
ACS Catal. 2015, 5, 1245−1253

REFERENCES

(1) Calegaro, M. L.; Lima, F. H. B.; Ticianelli, E. A. *J. Power Sources* **2006**, *158*, 735−739.
(2) Lima, F. H. B.; de Castro, J. F. R.; Ticianelli, E. A. *J. Power Sources* **2006**, *161*, 806−812.
(3) Alexeyeva, N.; Shulga, E.; Kisand, V.; Kink, I.; Tammeveski, K. *J. Electroanal. Chem.* **2010**, *648*, 169−175.
(4) Kruusenberg, I.; Matisen, L.; Shah, Q.; Kannan, A. M.; Tammeveski, K. *Int. J. Hydrogen Energy* **2012**, *37*, 4406−4412.
(5) Wu, J.; Zhang, D.; Wang, Y.; Wan, Y.; Hou, B. *J. Power Sources* **2012**, *198*, 122−126.
(6) Sarkar, A.; Manthiram, A. *J. Phys. Chem. C* **2010**, *114*, 4725−4732.
(7) Oezaslan, M.; Hasché, F.; Strasser, P. *J. Electrochem. Soc.* **2012**, *159*, B444−B454.
(8) van der Vliet, D.; Wang, C.; Debe, M.; Atanasoski, R.; Markovic, N. M.; Stamenkovic, V. R. *Electrochim. Acta* **2011**, *56*, 8695−8699.
(9) Neergat, M.; Rahul, R. *J. Electrochem. Soc.* **2012**, *159*, F234−F241.
(10) Yang, H.; Alonso-Vante, N.; Léger, J.-M.; Lamy, C. *J. Phys. Chem. B* **2004**, *108*, 1938−1947.
(11) Beard, B. C.; Ross, P. N. *J. Electrochem. Soc.* **1990**, *137*, 3368−3374.
(12) Qian, Y.; Wen; Adcock, P. A.; Jiang, Z.; Hakim, N.; Saha, M. S.; Mukerjee, S. *J. Phys. Chem. C* **2008**, *112*, 1146−1157.
(13) Soderberg, J. N.; Sirk, A. H. C.; Campbell, S. A.; Birss, V. I. *J. Electrochem. Soc.* **2005**, *152*, A2017−A2022.
(14) Lima, F. H. B.; de Castro, J. F. R.; Santos, L. G. R. A.; Ticianelli, E. A. *J. Power Sources* **2009**, *190*, 293−300.
(15) Ghosh, S.; Sahu, R. K.; Raj, C. R. *Nanotechnology* **2012**, *23*, 385602−385610.
(16) Wang, D.; Xin, H. L.; Wang, H.; Yu, Y.; Rus, E.; Muller, D. A.; DiSalvo, F. J.; Abruna, H. D. *Chem. Mater.* **2012**, *24*, 2274−2281.
(17) You, D. J.; Jin, S.-a.; Lee, K. H.; Pak, C.; Choi, K. H.; Chang, H. *Catal. Today* **2012**, *185*, 138−142.
(18) Sheng, W.; Lee, S. W.; Crumlin, E. J.; Chen, S.; Shao-Horn, Y. *J. Electrochem. Soc.* **2011**, *158*, B1398−B1404.
(19) Wang, D.; Xin, H. L.; Yu, Y.; Wang, H.; Rus, E.; Muller, D. A.; Abruna, H. D. *J. Am. Chem. Soc.* **2010**, *132*, 17664−17666.
(20) Yang, R.; Leisch, J.; Strasser, P.; Toney, M. F. *Chem. Mater.* **2010**, *22*, 4712−4720.
(21) Chen, H. M.; Liu, R.-S.; Lo, M.-Y.; Chang, S.-C.; Tsai, L.-D.; Peng, Y.-M.; Lee, J.-F. *J. Phys. Chem. C* **2008**, *112*, 7522−7526.
(22) Hou, L.; Qiu, H. *J. Power Sources* **2012**, *216*, 28−32.
(23) Zhou, X.; Gan, Y.; Du, J.; Tian, D.; Zhang, R.; Yang, C.; Dai, Z. *J. Power Sources* **2013**, *232*, 310−322.
(24) Shao, M.; Shoemaker, K.; Peles, A.; Kaneko, K.; Protsailo, L. *J. Am. Chem. Soc.* **2010**, *132*, 9253−9255.
(25) Wang, J. X.; Inada, H.; Wu, L.; Zhu, Y.; Choi, Y.; Liu, P.; Zhou, W.-P.; Adzic, R. R. *J. Am. Chem. Soc.* **2009**, *131*, 17298−17302.
(26) Mathew, P.; Meyers, J. P.; Srivastava, R.; Strasser, P. *J. Electrochem. Soc.* **2012**, *159*, B554−B563.
(27) Oezaslan, M.; Hasché, F.; Strasser, P. *J. Electrochem. Soc.* **2012**, *159*, B394−B405.
(28) Zhang, X.; Wang, H.; Key, J.; Linkov, V.; Ji, S.; Wang, X.; Lei, Z.; Wang, R. *J. Electrochem. Soc.* **2012**, *159*, B270−B276.
(29) Cochell, T.; Manthiram, A. *Langmuir* **2011**, *28*, 1579−1587.
(30) Strasser, P.; Koh, S.; Anniyev, T.; Greeley, J.; More, K.; Yu, C.; Liu, Z.; Kaya, S.; Nordlund, D.; Ogasawara, H.; Toney, M. F.; Nilsson, A. *Nat. Chem.* **2010**, *2*, 454−460.
(31) Wu, J.; Peng, Z.; Yang, H. *Philos. Trans. R. Soc., A* **2010**, *368*, 4261−4274.
(32) Xu, C.; Liu, Y.; Wang, J.; Geng, H.; Qiu, H. *ACS Appl. Mater. Interfaces* **2011**, *3*, 4626−4632.
(33) Bele, M.; Jovanovic, P.; Pavlisic, A.; Jozinovic, B.; Zorko, M.; Recnik, A.; Chernyshova, E.; Hocevar, S.; Hodnik, N.; Gaberscek, M. *Chem. Commun.* **2014**, *50*, 13124−13126.
(34) Hodnik, N.; Bele, M.; Hočevar, S. *Electrochem. Commun.* **2012**, *23*, 125−128.
(35) Komatsu, T.; Tamura, A. *J. Catal.* **2008**, *258*, 306−314.
(36) Lira, A.; Tailleur, R. G. *Fuel* **2012**, *97*, 49−60.
(37) Melo, L.; Velasquez, D.; Llanos, A.; Garcia, L.; Giannetto, G.; Guisnet, M.; Magnoux, P.; Alvarez, F. *Catal. Lett.* **2002**, *78*, 57−63.
(38) Cao, X.; Wang, N.; Jia, S.; Shao, Y. *Anal. Chem.* **2013**, *85*, 5040−5046.
(39) Coleman, E. J.; Co, A. C. *J. Catal.* **2014**, *316*, 191−200.
(40) Koh, S.; Strasser, P. *J. Am. Chem. Soc.* **2007**, *129*, 12624−12625.
(41) Markovic, N. M.; Gasteiger, H. A.; Ross, P. N. *J. Phys. Chem.* **1996**, *100*, 6715−6721.
(42) Holewinski, A.; Linic, S. *J. Electrochem. Soc.* **2012**, *159*, H864−H870.
(43) Damjanovic, A.; Genshaw, M. A. *Electrochim. Acta* **1970**, *15*, 1281−1283.
(44) Zhutaeva, G. V.; Tarasevich, M. R. *Prot. Met. Phys. Chem. Surf.* **2010**, *46*, 215−221.
(45) Stamenkovic, V. R.; Fowler, B.; Mun, B. S.; Wang, G.; Ross, P. N.; Lucas, C. A.; Marković, N. M. *Science* **2007**, *315*, 493−497.
(46) Gasteiger, H. A.; Kocha, S. S.; Sompalli, B.; Wagner, F. T. *Appl. Catal., B* **2005**, *56*, 9−35.
(47) Conway, B. E. *Prog. Surf. Sci.* **1995**, *49*, 331−452.

DOI: 10.1021/cs501762g
ACS Catal. 2015, 5, 1245−1253